LAGRANGIAN DATA ASSIMILATION FOR RIVER HYDRAULICS SIMULATIONS

Marc Honnorat*, Jérôme Monnier* and François-Xavier Le Dimet*

*Laboratoire de Modélisation et Calcul
B.P. 53, 38041 Grenoble Cedex 9, France
e-mail: marc.honnorat@imag.fr
web page: http//www-lmc.imag.fr

Key words: Data assimilation, River hydraulics, Lagrangian data, Parameter identification

Abstract. *We present a method to use lagrangian data from remote sensing observation in a data assimilation process for parameters identification in a river hydraulics model based on the bidimensional shallow water equations. The trajectories of particles advected by the flow can be extracted from video images and are used in addition to classical eulerian observations. This lagrangian data bring information on the surface velocity thanks to an appropriate transport model. Numerical twin data assimilation experiments demonstrate that this method makes it possible to significantly improve the identification of bed elevation and initial conditions.*

1 INTRODUCTION

The numerical simulation of river flows requires a precise modelling of the underlying physics. The bidimensional shallow water equations can describe accurately many free surface hydraulic configurations. In order to carry out a realistic simulation of a particular system, numerical models require information on physical parameters such as bed elevation, roughness coefficients in addition to initial and boundary conditions. Unfortunately, many model parameters are usually not well known and must be calibrated. Since the quality of the simulation is largely dependent on these model inputs, the later must be defined accurately.

To improve the quality of the simulation, data assimilation methods combine optimally information from the model and observation data in order to identify the value of model parameters consistent with reality. Variational data assimilation [1] consists in minimizing a cost function that measures the discrepancy between simulation results and physical measurements. The minimization is performed by a quasi-Newton method [2], which requires the computation of the gradient of the cost function. The latter can be efficiently computed using the solution to an adjoint model.

However, in river hydraulics, observation data are available only in very small quantities. River water level can be measured locally at gauging stations, but such observations are usually very sparse in space. Velocity measurements are even more scarce, since they usually require complex human interventions. Consequently, the available eulerian observations are not sufficient to take full advantage of data assimilation for many identification problems.

Therefore, new kinds of observations would bring additional information on the flow. In particular, remote sensing techniques make it possible to get information on the water surface. We present a method to use lagrangian data, which can be extracted from video images, into the assimilation process. We consider observations of particles spread on the water surface and advected by the flow. The link between the shallow water model and the trajectories of these particles is made thanks to an appropriate transport model. To use this information in the data assimilation process, we introduce a cost function measuring the distance between the trajectory of model particles and the available observations. The lagrangian data is used in addition to classical eulerian observations of water depth.

When considering real flows, the water surface is perturbed by physical phenomena that cannot be represented in the model. To cope with this difficulty, an observation operator based on a multi-scale filtering scheme is proposed to remove small-scale perturbations from trajectories observations.

Lagrangian data assimilation is applied to the identification of bed elevation and initial conditions for an academic configuration of a river hydraulics model based on the shallow water equations. The discretization of the direct shallow water model rely on the finite volume method and the HLLC [3] approximate Riemann solver. The adjoint model is written using automatic differentiation tool Tapenade [4]. Numerical twin data assimilation experiments demonstrate that the proposed method makes it possible to improve significantly the quality of the identification.

The bidimensional conservative shallow water equations are introduced in Section 2 and the variational data assimilation procedure for lagrangian data is described in Section 3. The discretization of the direct model, the numerical scheme for the computation of trajectories and the implementation of the adjoint model are presented in Section 4. A filter used to smooth observations of trajectories is introduced in Section 5. Finally, twin experiments and numerical results of data assimilation for the identification of bed elevation and initial conditions are presented in Sections 6 and 7.

2 SHALLOW WATER MODEL

The river hydraulics model considered rely on the bidimensional shallow water equations in a conservative formulation. The state variables are the water depth h and the local discharge $\mathbf{q} = h\mathbf{u}$, where $\mathbf{u}$ is the depth-averaged velocity vector. On a domain Ω and for a computational time interval $[0, T]$, the shallow water equations associated with

initial and boundary conditions can be written as

$$
\begin{cases}
\partial_t\, h + \mathrm{div}(\mathbf{q}) \;=\; 0 & \text{in } \Omega\times\,]\,0,T] \\[4pt]
\partial_t\, \mathbf{q} + \mathrm{div}(\tfrac{1}{h}\mathbf{q}\otimes\mathbf{q}) + \tfrac{1}{2}g\nabla h^2 + gh\nabla z_b + g\frac{n^2\|\mathbf{q}\|}{h^{7/3}}\mathbf{q} \;=\; 0 & \text{in } \Omega\times\,]\,0,T] \\[4pt]
\underline{\text{I.C.}} \quad h(0) \;=\; h_0\,, \quad \mathbf{q}(0) \;=\; \mathbf{q}_0\,, \\[4pt]
\underline{\text{B.C.}} \quad (\mathbf{q}\cdot\mathbf{n})|_{\Gamma_q} \;=\; -\bar q\,, \quad (\mathbf{q}\cdot\mathbf{n})|_{\Gamma_w} \;=\; 0\,, \quad h|_{\Gamma_z} \;=\; \bar z_s - z_b|_{\Gamma_z}\,, \\[4pt]
\qquad\quad (\partial_{\mathbf{n}} h)|_{\Gamma_q\cup\Gamma_w\cup\Gamma_t} \;=\; 0\,, \quad (\partial_{\mathbf{n}}\mathbf{q})|_{\Gamma_t} \;=\; 0\,, \quad \partial_{\mathbf{n}}(\mathbf{u}\cdot\mathbf{n}+2c)|_{\Gamma_z} \;=\; 0
\end{cases}
\tag{1}
$$

where g is the magnitude of the gravity, z_b the bed elevation, n the Manning roughness coefficient, h_0 and $\mathbf{q}_0$ the initial conditions for the state variables. The variable $c = \sqrt{gh}$ denotes the local wave celerity.

The boundary Γ of the domain Ω is split up as $\Gamma = \Gamma_q \cup \Gamma_z \cup \Gamma_w \cup \Gamma_t$ for four different kinds of boundary conditions.

- Γ_q: a scalar discharge $\bar q$ is prescribed
- Γ_z: a water elevation $\bar z_s$ is prescribed
- Γ_w: a slip condition on the velocity is prescribed
- Γ_t: homogeneous Neumann conditions for all state variables are prescribed.

The model state variables $(h, \mathbf{q})$ are completely determined by the value of the control vector $\mathbf{c} = (h_0, \mathbf{q}_0, n, z_b, \bar q, \bar z_s)$.

3 LAGRANGIAN DATA ASSIMILATION

Variational data assimilation [1] is based on optimal control theory [5] and consists in identifying the control vector $\mathbf{c}$ that minimizes a cost function measuring the discrepancy between the state variable of the model and data obtained from the observation of the physical system. An efficient minimization of the cost function is carried out a quasi-Newton method that requires the computation of its gradient. We use the M1QN3 algorithm [2] based on the BFGS formula.

Lagrangian data assimilation consists in using observations described by lagrangian coordinates in the data assimilation process. Here, we consider observations of particles transported by the flow. However, the state of the flow is described in eulerian coordinates by the shallow water model. The link between the lagrangian data made of particle trajectories and the classical eulerian variables of the shallow water model is made by an appropriate transport model.

3.1 Transport model

Let us consider a set of N particles transported by the flow. We state that their trajectories $X_i(t)$ are solutions of the following ODEs:

$$
\begin{cases}
\frac{d}{dt}X_i(t) \;=\; \gamma\,\mathbf{u}\big(X_i(t),t\big) & \forall\, t \in\,]t_i^0, t_i^f[\\[4pt]
X_i(t_i^0) \;=\; x_i^0\,,
\end{cases}
\qquad \text{for } i = 1,\dots,N
\tag{2}
$$

where t_i^0 and t_i^f are the time when the particle enter and leave the observation domain. The particles are transported by a velocity that is related to the shallow water model velocity by a multiplicative constant γ. This set of ODEs is weakly coupled with the shallow water model since the state variable of the latter is not dependent on the solution of the former.

3.2 Observations and cost function

We consider two kinds of observations. The first one consists in classical, eulerian observations of the water depth in some locations of the physical domain, denoted by $h^{obs}(t)$. The second kind consists in the trajectories of physical particles transported by the water flow. These lagrangian observations are denoted by $X_i^{obs}(t)$.

In order to take into account both kinds of observations, we build a composite cost function measuring the discrepancy between observation data and model state variables:

$$j(\mathbf{c}) \;=\; \frac{1}{2}\int_0^T \left\| Ch(t) - h^{obs}(t) \right\|^2 dt \;+\; \frac{\alpha_t}{2}\sum_{i=1}^N \int_{t_i^0}^{t_i^f} \left| X_i(t) - X_i^{obs}(t) \right|^2 dt \,, \qquad (3)$$

where $\mathbf{c} = (h_0, \mathbf{q}_0, n, z_b, \bar{q}, \bar{z}_s)$ is the control vector, α_t a scaling parameter, C the observation operator that map the model variables to the space of eulerian observations. The first term measures the discrepancy between water depth observations and model state variable. The second term measures the distance between virtual particles of the transport model and observations of trajectories.

3.3 Adjoint model

The adjoint method makes it possible to compute efficiently all partial derivatives of the cost function j with respect to the components of the control vector $\mathbf{c}$. We introduce the following weakly coupled adjoint model set.

$$\begin{cases} \text{For } i = 1, \dots, N \\[4pt] \quad \frac{d}{dt}\widetilde{X}_i(t) + \gamma[\nabla\mathbf{u}]^T\,\widetilde{X}_i = \alpha_t\left(X_i(t) - X_i^{obs}(t)\right) \qquad \forall t \in \,]t_i^0, t_i^f[\\[4pt] \quad \widetilde{X}_i(t) \;=\; 0 \qquad\qquad\qquad\qquad\qquad\qquad\qquad \forall t \in \,]0, t_i^0]\cup[t_i^f, T[\end{cases} \qquad (4)$$

$$\begin{cases} \partial_t\widetilde{h}(t) - \left[(\mathbf{u}\cdot\nabla)\,\widetilde{\mathbf{q}}\right]\cdot\mathbf{u} + gh\,\mathrm{div}(\widetilde{\mathbf{q}}) - g\,\widetilde{\mathbf{q}}\cdot\nabla z_b + \frac{7}{3}g\frac{n^2\|\mathbf{u}\|}{h^{4/3}}\mathbf{u}\cdot\widetilde{\mathbf{q}} \\[4pt] \qquad\qquad = \frac{\gamma}{h}\sum_{i=1}^N \mathbf{u}\cdot\widetilde{X}_i(t) + C^T\!\left(Ch(t) - h^{obs}(t)\right) \qquad \forall t \in \,]0, T[\\[4pt] \partial_t\widetilde{\mathbf{q}}(t) + \nabla\widetilde{h} + (\mathbf{u}\cdot\nabla)\,\widetilde{\mathbf{q}} + (\nabla\widetilde{\mathbf{q}})^T\mathbf{u} - g\frac{n^2\|\mathbf{u}\|}{h^{4/3}}\widetilde{\mathbf{q}} \\[4pt] \qquad\qquad - g\frac{n^2}{h^{4/3}\|\mathbf{u}\|}(\mathbf{u}\otimes\mathbf{u})\widetilde{\mathbf{q}} \;=\; -\frac{\gamma}{h}\sum_{i=1}^N \widetilde{X}_i(t) \qquad\qquad \forall t \in \,]0, T[\\[4pt] \underline{\text{I.C.}}\quad \widetilde{h}(T) \;=\; 0, \quad \widetilde{\mathbf{q}}(T) \;=\; 0, \\[4pt] \underline{\text{B.C.}}\quad \widetilde{\mathbf{q}}|_{\Gamma_q} = 0, \quad (\widetilde{\mathbf{q}}\cdot\mathbf{n})|_{\Gamma_w} = 0, \quad \widetilde{\mathbf{q}}|_{\Gamma_t} = 0, \quad (\widetilde{\mathbf{q}}\cdot\tau)|_{\Gamma_z} = 0, \\[4pt] \qquad (\partial_{\mathbf{n}}\widetilde{h})|_{\Gamma_q\cup\Gamma_w} = 0, \quad \widetilde{h}|_{\Gamma_t} = 0, \quad \left(\widetilde{h} + 2(\mathbf{u}\cdot\mathbf{n})(\widetilde{\mathbf{q}}\cdot\mathbf{n})\right)|_{\Gamma_z} = 0 \end{cases} \qquad (5)$$

4

A backward integration in time of the adjoint transport model (4) followed by a backward integration in time of the adjoint shallow water model (5) give a solution $(\widetilde{X}, \widetilde{h}, \widetilde{\mathbf{q}})$ to the weakly coupled system. Then, the partial derivatives of the cost function are simple functions of the adjoint state variables $\widetilde{h}$ and $\widetilde{\mathbf{q}}$. For example, we have

$$\frac{\partial j}{\partial h_0}(\mathbf{c}) = -\widetilde{h}(0)\,, \quad \frac{\partial j}{\partial \mathbf{q_0}}(\mathbf{c}) = -\widetilde{\mathbf{q}}(0)\,, \quad \frac{\partial j}{\partial z_b}(\mathbf{c}) = -\int_0^T \mathrm{div}\Big(gh(t)\widetilde{\mathbf{q}}(t)\Big)\, dt\,,$$
$$\frac{\partial j}{\partial \bar{q}}(\mathbf{c}) = -\widetilde{h}|_{\Gamma_q}, \quad \frac{\partial j}{\partial \bar{z}_s}(\mathbf{c}) = \Big[(\widetilde{\mathbf{q}}\cdot\mathbf{n})\big(c^2 - (\mathbf{u}\cdot\mathbf{n})^2\big)\Big]\big|_{\Gamma_z}\,.$$

These partial derivatives are used as inputs to the minimization algorithm. A single integration of the direct model (1)–(2) followed by a single integration backward in time of the adjoint model (4)–(5) are sufficient to compute all components of the gradient of the cost function.

4 DISCRETIZATION

4.1 Finite Volume solver

The bidimensional shallow water equations described in Section 2 are solved numerically on a structured mesh using the finite volume method. The system (1) can be written in a general form as

$$\partial_t U \;+\; \mathrm{div}\, F(U) \;=\; S(U)\,, \tag{6}$$

where $U = (h, \mathbf{q})^T$ is the vector of conservative variables, $F(U) = \big(G(U), H(U)\big)^T$ the flux vector and $S(U)$ the source term

$$G(U) = \begin{pmatrix} q_x \\ \frac{1}{h}q_x^2 + \frac{1}{2}gh^2 \\ \frac{1}{h}q_x q_y \end{pmatrix}, \; H(U) = \begin{pmatrix} q_y \\ \frac{1}{h}q_x q_y \\ \frac{1}{h}q_y^2 + \frac{1}{2}gh^2 \end{pmatrix}, \; S(U) = \begin{pmatrix} 0 \\ -gh\nabla z_b - g\frac{n^2\|\mathbf{q}\|_2}{h^{7/3}}\,\mathbf{q} \end{pmatrix}\,.$$

The computational domain Ω is discretized using quadrangular cells. We define the mean value of the state variable U on an arbitrary cell K_i by

$$U_i = \frac{1}{|K_i|}\int_{K_i} U\, d\Omega\,,$$

where $|K_i|$ denotes the surface of the cell. By integrating (6) over K_i, using the divergence theorem, we obtain

$$\int_{K_i} \partial_t U\, d\Omega \;+\; \sum_{j=1}^{N_i} \int_{E_{ij}} T_{ij}^{-1} G(T_{ij}U)\, ds \;=\; \int_{K_i} S(U)\, d\Omega\,,$$

where N_i denotes the number of faces of the cell K_i (3 or 4), E_{ij} is the cell interface (see Fig. 1) and T_{ij} is the 3×3 rotation matrix of angle θ_{ij}. The usual flux term derived from
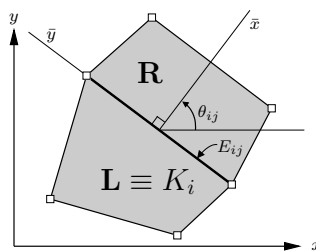
Figure 1: Two adjacent finite volumes.

the divergence theorem has been replaced by integrals over the cell edges thanks to the rotational invariance property of the shallow water equations (see [3, p. 65]). Hence, the bidimensional problem actually consists in a sum of one-dimensional Riemann problems that can be solved numerically using a Riemann solver. One can write the following semi-discrete scheme

$$\frac{d}{dt}U_i \; + \; \frac{1}{|K_i|}\sum_{j=1}^{N_i} T_{ij}^{-1}\,\widetilde{G}(U_L, U_R) = S_i \; , \tag{7}$$

where $\widetilde{G}(U_L, U_R)$ is an approximation of the flux through the cell interface E_{ij}. Subscripts L and R denote cells respectively to the left and to the right of the interface. To compute numerically the discrete flux $\widetilde{G}(U_L, U_R)$, we use the HLLC approximate Riemann solver [3]. The discretization of the bed slope is actually included in the flux term. A forward Euler scheme is used for time discretization. The following stability condition on the time step Δt must be satisfied: $\Delta t \leq \frac{\min(d_{L,R})}{\max(\|\mathbf{u}\|+c)}$, where $d_{L,R}$ is the distance between the cell center and the center of interface.

4.2 Trajectories

The trajectories of the particles are obtained by the integration of (2) using a second-order Runge-Kutta scheme. Let $(t_n)_n$ be a subdivision of the time interval $[t_i^0, t_i^f[$ and let $\Delta t_n = t_{n+1} - t_n$. To compute an approximation X_i^n of the solution $X_i(t_n)$ to the transport model (2), we use the second-order time integration scheme

$$\begin{aligned}
X_i^0 \;&=\; x_i^0 \; , \\
&\underline{\text{For } n = 0, \dots :} \\
&\left\{
\begin{array}{rcl}
X_i^{n,1} &=& X_i^n + \Delta t_n\,\gamma\,\mathbf{u}\big(X_i^n, t_n\big) \\
X_i^{n,2} &=& X_i^n + \Delta t_n\,\gamma\,\mathbf{u}\big(X_i^{n,1}, t_{n+1}\big) \\
X_i^{n+1} &=& \frac{1}{2}\big(X_i^{n,1} + X_i^{n,2}\big)
\end{array}
\right.
\end{aligned} \tag{8}$$

This scheme needs the value of the velocity $\mathbf{u}$ for an arbitrary position $P = (p_x, p_y)$ in the domain Ω. Since the velocity field is known only as a discrete finite volume solution to the

shallow water equations, we use an interpolation to compute an approximation $\mathbf{u}_P(t_n)$ of $\mathbf{u}(P, t_n)$. Figure 2 shows a part of a structured, rectangular mesh of the computational domain. The velocity $\mathbf{u}$ is known at each computational time t_n by an approximation
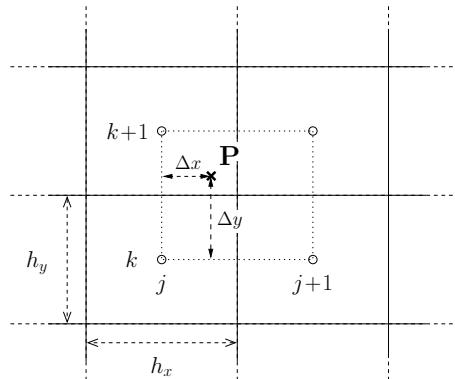

Figure 2: Interpolation grid for the velocity field.

of its mean value on each cell $K_{j,k}$ denoted by $\mathbf{u}_{j,k}^n$. Using the notations of Figure 2, we introduce the following interpolation scheme

$$
\begin{aligned}
\mathbf{u}_P(t_n) \;=\; \tfrac{1}{h_x h_y} \Big(& (h_x - \Delta x)(h_y - \Delta y)\, \mathbf{u}_{j,k}^n + \Delta x \Delta y\, \mathbf{u}_{j+1,k+1}^n \\
& + \Delta x\,(h_y - \Delta y)\, \mathbf{u}_{j+1,k}^n + (h_x - \Delta x)\Delta y\, \mathbf{u}_{j,k+1}^n \Big)
\end{aligned}
\tag{9}
$$

Since the mesh is structured and the cells are rectangular, this scheme is second-order accurate.

4.3 Adjoint model

In practice, there are three main methods to obtain an implementation of the adjoint model. The continuous adjoint model (5) can be discretized using an appropriate numerical scheme which is then implemented. A major difficulty relies on the fact that the adjoint equations are not in a conservative form, therefore the numerical scheme used for the direct equations cannot be applied. A second solution consists in writing the adjoint of the direct numerical scheme and implement it. Actually, we use a better way that consists in writing directly the adjoint code of the implementation of the direct model. A large part of this extensive task can be automated using algorithmic differentiation [6]. Here, the direct program is coded in Fortran 90 and we use the automatic differentiation tool Tapenade [4].

The direct and adjoint codes are included in a sofware called Dassflow [7] designed to carry out data assimilation experiments.

5   TRAJECTORY FILTERING

When we consider real flows, surface velocity is perturbed by many physical phenomena that are not taken into account neither in the shallow water model nor in the particle transport model. Therefore, if a large number of trajectories observations is available, it should be profitable to filter this information in order to remove small-scale perturbations from the data set. Such a filter based on *a priori* information on the flow can improve the quality of data assimilation and consequently the quality of parameter identification.

In the proposed method, filtered trajectories are reconstructed from a local average in time and space of the velocity field. We seek to create a set $\left\{X_j^m\right\}_{j=1,N_m}$ of trajectories defined as

$$\begin{cases} \frac{d}{dt}X_j^m(t) & = & \mathbf{u}^m\big(X_j^m(t),t\big) \qquad \forall\, t \in \,]t_j^0, t_j^f[\\ X_j^m(t_j^0) & = & x_j^0 \end{cases} . \tag{10}$$

where $\mathbf{u}^m$ is the local average velocity and x_j^0 the starting point of the filtered trajectory j. Let $\mathbf{u}^{m,j}(t) = \mathbf{u}^m\big(X_j^m(t),t\big)$ denote the velocity of filtered particle j at time t. It is computed as the mean velocity observed at time t on a time-space window $\mathcal{W} = \mathcal{W}_t \times \mathcal{W}_{X_j^m(t)}$, where $\mathcal{W}_t$ denotes a temporal neighborhood of t and $\mathcal{W}_{X_j^m(t)}$ a spatial neighborhood of $X_j^m(t)$. Using these notations, we define

$$\mathbf{u}^{m,j}(t) \;=\; \frac{1}{\mathbb{W}_t^j}\sum_{i=1}^{N_{obs}} \int_{\mathcal{W}_t} \frac{d}{ds}X_i^{obs}(s)\,\mathbb{1}_{X_i^{obs}(s)\in\mathcal{W}_{X_j^m(t)}}\;ds\;, \tag{11}$$

where

$$\mathbb{W}_t^j = \sum_{i=1}^{N_{obs}} \int_{\mathcal{W}_t} \mathbb{1}_{X_i^{obs}(s)\in\mathcal{W}_{X_j^m(t)}}\;ds\;.$$

On Figure 3 is drawn a square spatial window for a particle located in X^m at time t. Two raw trajectories of observed particles are represented with dotted lines. The solid lines correspond to the part of the trajectories included in the time window $\mathcal{W}_t$ while the bold lines match the intersection of the latter with the space window, *i.e.* the parts of
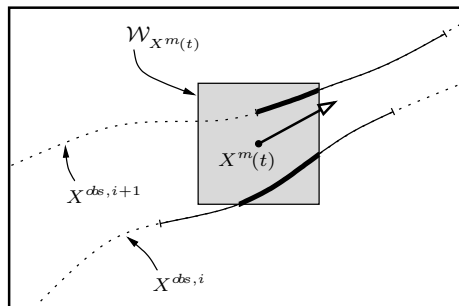

Figure 3: Space and time windows for trajectories filtering.

the trajectories actually taken into account in the computation of the local mean velocity $\mathbf{u}^{m,j}(t)$. The filtered trajectories X_j^m are used instead of the raw observations X_i^{obs} in the data assimilation process.

6 TWIN EXPERIMENTS

6.1 Description

Twin experiments consist in data assimilation experiments where the observations are created by the model with a given set of parameters. This makes it possible to evaluate a data assimilation method with a complete knowledge of all parameters, with no dependence on external variables.

A reference simulation is performed using a known set of parameters $\mathbf{c}^{ref}$. The resulting state variables, called h^{ref} and $\mathbf{u}^{ref}$ are used to create observations. Here, we will consider observations of water depth, denoted by h^{obs} and observations of trajectories, denoted by X^{obs}.

Then, a different configuration resulting from a modified set of parameters $\tilde{\mathbf{c}}$ made of *a priori* hypotheses on the reference flow is used as an initial guess for a data assimilation experiment. The aim is to identify the reference set of parameters $\mathbf{c}^{ref}$ using the synthetic observations.

In order to evaluate the quality of the identification, we introduce a diagnostic function j_{tot} measuring the discrepancy between the reference state variable and a simulation resulting from an arbitrary parameter vector $\mathbf{c}$.

$$j_{tot}(\mathbf{c}) = \frac{1}{2} \int_0^T \left(\left\| h(t) - h^{ref}(t) \right\|_\Omega^2 + \left\| \mathbf{u}(t) - \mathbf{u}^{ref}(t) \right\|_\Omega^2 \right) dt \qquad (12)$$

If the observations are perfect, directly derived from the model state variables with no additional noise, then $j_{tot}(\mathbf{c}^{ref}) = 0$.

6.2 Perturbation of trajectories

For the numerical twin experiment, we will actually construct observations of perturbed trajectories, *i.e.* trajectories of particles transported by a turbulent velocity field denoted by $\mathbf{u}^t$. We consider a simple perturbation model where the observations consist in trajectories of particles transported by a velocity field made up of the sum of the model velocity $\gamma\mathbf{u}$ and a perturbation $\mathbf{u}^p$.

$$\mathbf{u}^t(x,t) = \gamma\mathbf{u}(x,t) + \mathbf{u}^p(x,t) . \qquad (13)$$

We define the perturbation $\mathbf{u}^p$ as a Gauss-Markov stochastic process. Let the random variable $\mathbf{u}_n^p = \mathbf{u}^p(\cdot, t_n)$ denote the perturbation velocity field at time t_n. We introduce the Reynolds tensor $R(t_n)$ and the time correlation tensor $\Lambda(t_n, t_m)$ defined as

$$R(t_n) = \mathbb{E}\left(\mathbf{u}_n^p \, \mathbf{u}_n^{p\,T} \right)$$
$$\Lambda(t_n, t_m) = \mathbb{E}\left(\mathbf{u}_n^p \, \mathbf{u}_m^{p\,T} \right) .$$

The perturbation $\mathbf{u}_n^p$ is defined recursively by the following recursive equation

$$\mathbf{u}_{n+1}^p = \Lambda(t_{n+1}, t_n)R^{-1}(t_n)\mathbf{u}_n^p + \mathbf{v}_n ,$$

where $\mathbf{v}_n$ is a random variable with a zero-mean gaussian distribution and a covariance matrix V_n defined by

$$V_n = R(t_{n+1}) - R^{-1}(t_n)\Lambda^2(t_{n+1}, t_n) .$$

We will consider the particular case where the Reynolds tensor R does not depend on time and where the time correlation tensor Λ is an exponentially decreasing function in time.

$$R(t_{n+1}) = R(t_n) = R$$

$$\Lambda(t_n + \Delta t_n, t_n) = e^{-\frac{\Delta t_n}{T_{L_n}}}R ,$$

where T_{L_n} is the local turbulence characteristic duration at time t_n and R is a symmetric positive-definite matrix. With these additional assumptions, we have the following expressions

$$V_n = \left(1 - e^{-\frac{2\Delta t_n}{T_{L_n}}}\right) R \tag{14}$$

$$\mathbf{u}_{n+1}^p = e^{-\frac{\Delta t_n}{T_{L_n}}}\mathbf{u}_n^p + \mathbf{v}_n \tag{15}$$

7 NUMERICAL RESULTS

We present results of twin experiments carried out to evaluate lagrangian data assimilation. Observations of particle trajectories are used in combination with local water depth measurements, first for the identification of the bed elevation z_b as the only control variable and for the joint identification of z_b and the initial conditions h_0 and $\mathbf{u}_0$ in a second time.

7.1 Flow configuration

We consider a $100 \times 16\,m$ rectangular channel. The bed has a longitudinal slope of 0.4% and features a bump spanned on the whole width, centered in $x = 40\,m$ with an amplitude of $0.25\,m$ and a length of $30\,m$. This bump generates an acceleration of the flow in the region $x \in [25, 60]$.

A constant discharge $\bar{q} = 8\,m^3/s$ is prescribed at the boundary $\Gamma_q :\ x = 0\,m$. The boundaries $y = 0$ and $y = 16\,m$ are defined as walls and denoted by Γ_w. Finally, Neumann conditions are prescribed on the boundary $\Gamma_t :\ x = 100\,m$ (see Figure 4 (a)). In order to simulate boundary layer effects, the value of the Manning coefficient n is variable in space. In the central part of the domain, denoted by Ω_1 and defined by $|y - 8| < 4\,m$, n is set to 0.02. In the complement of Ω_1 in Ω, *i.e.* the lateral sides of the domain, denoted

by Ω_2, the value of n increases linearly from 0.02 at the intersection with Ω_1 up to 0.04 at the boundary Γ_w.

These conditions drive the flow to a steady state that is used as an initial condition for the twin experiments. A vertical cut of the fluid domain in the longitudinal plane in Figure 4 (b) shows the bed and the free surface elevation for this configuration. Twin data
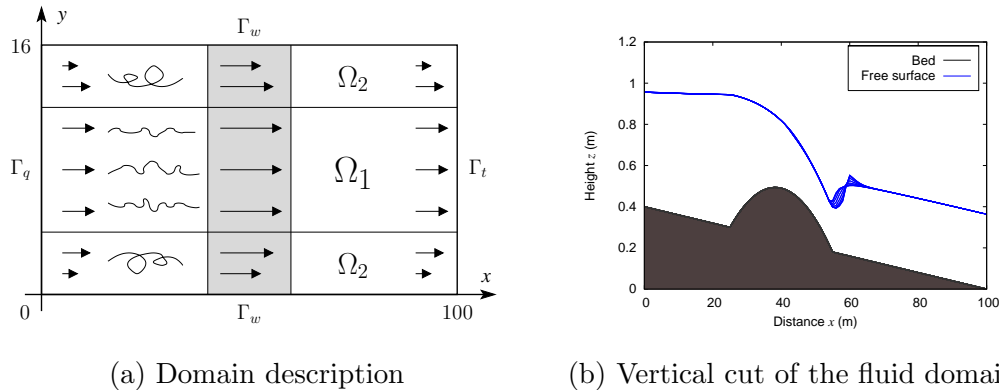

(a) Domain description   (b) Vertical cut of the fluid domain

Figure 4: Twin experiments flow configuration

assimilation experiments are carried out for a simulation time $T = 100\,s$ and a constant time step $\Delta t = 0.1\,s$.

7.2 Creation of observations

Observations are created by the model from the reference steady flow described above. Water depth is recorded continuously in time at the abscissae $x_1 = 15\,m$ and $x_2 = 70\,m$, for the whole width of the domain. These measurements are used as observations denoted by $h_i^{obs}(y; t)$ for $i = 1, 2$ in the twin experiments.

For the creation of trajectories observations, virtual particles are dropped in the reference steady flow near boundary Γ_q and transported by a turbulent surface velocity $\mathbf{u}^t = \gamma \mathbf{u} + \mathbf{u}^p$, where $\gamma = 1$ and $\mathbf{u}^p$ is a Gauss-Markov process as described in section 6.2. The correlation matrix R can be written as

$$R = \begin{pmatrix} \sigma_1^2 & \rho \sigma_1 \sigma_2 \\ \rho \sigma_1 \sigma_2 & \sigma_2^2 \end{pmatrix}$$

with standard deviations σ_1 and σ_1 defined as

$$\sigma_1 = \sqrt{\frac{c_1}{1 + \mathbf{u}_1^2}} \qquad \text{and} \qquad \sigma_2 = \sqrt{\frac{c_2}{1 + \mathbf{u}_2^2}} \quad .$$

This choice corresponds to a perturbation that lessen when the magnitude of the velocity increases. The numerical value of the parameters depends on the position in the domain. They are summarized in Table 1. A set of 32 particles are released in the flow,
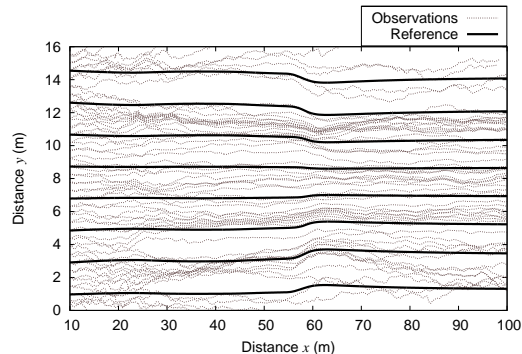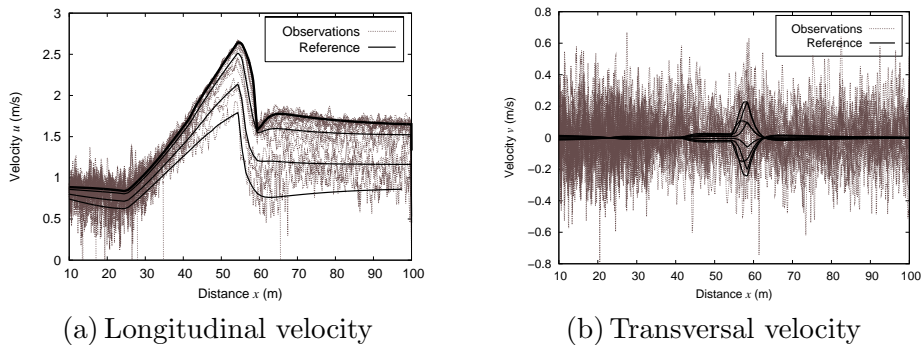
Figure 5: Trajectories of particles transported by a turbulent surface velocity field.

every 2 seconds of simulation, uniformly distributed over the width of the channel at the point $x = 10\,m$. Altogether, we take into account $N_{obs} = 640$ particles. The trajectories of these particles transported by the turbulent velocity field $\mathbf{u}^t$ are used as raw observations, denoted by X_i^{obs}. They are drawn with dotted lines in Figure 5. Reference trajectories of particles that would be transported by an undisturbed velocity field (where $\mathbf{u}^p \equiv 0$) are drawn in bold continuous lines. Such reference trajectories will be denoted by X_i^{ref} in the following. In the same way, the longitudinal and transversal velocities are traced respectively in Figures 6 (a) and 6 (b).

(a) Longitudinal velocity

(b) Transversal velocity

Figure 6: Velocities of particles transported by a turbulent surface velocity field.

	ρ	c_1	c_2	T_L
domain Ω_1	0.2	0.5	0.3	0.6
domain Ω_2	0.3	0.6	0.4	0.3

Table 1: Values of Gauss-Markov process parameters.

7.3 Trajectories filtering

Filtered trajectories are reconstructed from the observed trajectories X_i^{obs} using filters with different scales. From the *a priori* hypothesis that the flow is stationary, we choose the largest possible time window $\mathcal{W}_t = [0, T]$ for all time t.

The dimensions of the space window should be chosen in order to be large enough to remove small-scale perturbations, yet small enough to prevent from smoothing most important characteristics of the flow. Since the flow features large longitudinal variations, the corresponding dimension of the space window is set to 1% of the domain length, *i.e.* $1\,m$. Concerning the transversal dimension, a filter width equal to the size of the domain would remove boundary layer effects. On the other hand, a too small value would not smooth enough transversal perturbations. A good compromise has been found with $\frac{1}{16}$ of the channel width, *i.e.* $1\,m$. A total of 200 filtered trajectories are reconstructed using sets of 10 particles released in the flow every 2 seconds, uniformly distributed over the width of the channel at the point $x = 10\,m$.

7.4 Identification of topography

We seek to identify the reference topography used to create the observations, from the *a priori* hypothesis that the bed is made of a longitudinal slope of 0.4% without bump. To that purpose, we carry out data assimilation using the available observations, *i.e.* water depth measurements and particle trajectories. In this experiment, the only modified parameter when compared to the reference flow is the bed topography z_b. In particular, the initial condition remains unchanged.

7.4.1 Water depth measurements

We first try to identify the topography using only water depth measurements h_i^{obs} at the abscissae $x_1 = 15\,m$ and $x_2 = 70\,m$. The corresponding cost function is the following

$$j_1(z_b) \;=\; \frac{1}{2}\sum_{i=1}^{2}\int_0^T\int_0^{y_{max}}\left\|h(x_i, y; t) - h_i^{obs}(y; t)\right\|^2 dy\, dt \;+\; \frac{\alpha_p}{2}\left\|\nabla z_b\right\|^2 . \qquad (16)$$

A regularization term involving the norm of the topography gradient is introduced in the cost function in order to smooth the solution. The parameter α_p is the weight of this penalization with respect to the observations. In this experiment, it set to the value $\alpha_p = 10^{-4}$.

In this configuration, the minimization algorithm converges very slowly to an identified topography that is not very satisfactory when compared to the reference. Figure 7 (a) presents the reference topography in a bold solid line as well as the identified one with a fine grey line. We can see that the latter comprises large variations with respect to the reference before the bump. The evolution of the cost function, the norm of its gradient and the value of the diagnostic function j_{tot} are shown in Figure 7 (b). We can see that the

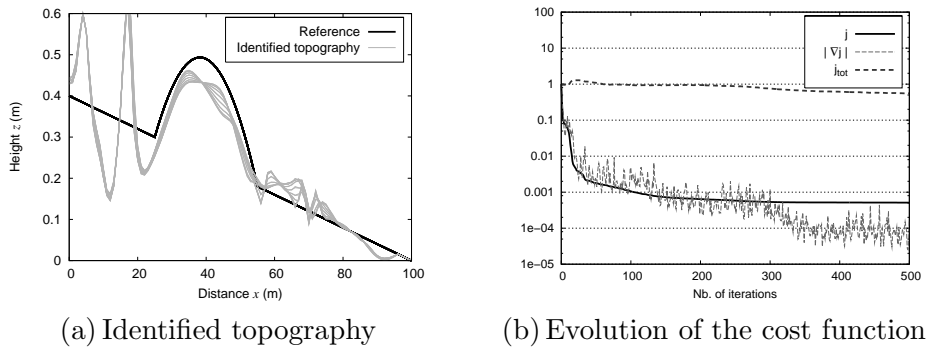(a) Identified topography

(b) Evolution of the cost function

Figure 7: Identification of the topography using water depth measurements. $\alpha_p = 10^{-4}$.

value of j_{tot} has not even be divided by 2, which means that the identification is globally far from being satisfactory.

7.4.2 Observation of reference trajectories

In this experiment, we add observations of the 640 reference trajectories X_i^{ref} to the water depth measurements. The particles are transported by the undisturbed shallow water velocity field, so this experiment will be used as a reference to evaluate the performance of the filtering process in the following sections.

The cost function is built from j_1 with an additional term measuring the distance between virtual particles and reference particles.

$$j_2(z_b) \;=\; j_1(z_b) \;+\; \frac{\alpha_t}{2} \sum_{i=1}^{N_{obs}} \int_0^T \left| X_i(t) - X_i^{ref}(t) \right|^2 \, dt \; , \tag{17}$$

where α_t is the weight given to the observations of trajectories. It is set to $\alpha_t = 10^{-5}$, which roughly balances the value of the term associated to the water depth measurement and the one associated the observations of trajectories. The weight α_p remains set to 10^{-4}. As we can see in Figure 8 (a), the identified topography is very close to the reference. This observation is confirmed by the fact that the value of the diagnostic function j_{tot} is divided by 530 at the end of the optimization process. The quality of the identification is thus very good.

7.4.3 Observation of perturbed trajectories

In this experiment, we add observations of the 640 perturbed trajectories X_i^{obs} to the water depth measurements. The cost function is built from j_1 with an additional term measuring the distance between virtual particles and particles transported by the turbu-

lent velocity field.

$$j_3(z_b) \;=\; j_1(z_b) \;+\; \frac{\alpha_t}{2} \sum_{i=1}^{N_{obs}} \int_0^T \left| X_i(t) - X_i^{obs}(t) \right|^2 \, dt \qquad (18)$$

When using the same values for the parameters α_p and α_t as in section 7.4.2, the identified topography is very irregular with small-scale variations of large amplitude, as shown in Figure 9 (a). Nevertheless, the shape of the bump is roughly identified. As we can see in Figure 9 (b), the value of the diagnostic function j_{tot} decreases in a first time during the minimization process, but then increases up to a quarter of its initial value.

It is possible to obtain slightly better results by increasing substantially the weight α_p of the regularization term. For instance, with $\alpha_p = 10^{-2}$, the final value of j_{tot} is divided by 7 with respect to its initial value instead of 4. However, the identified topography is too much smoothed when compared to the reference.

7.4.4   Observation of filtered trajectories

We now use the filtered trajectories X_j^m as observations. The cost function is built from j_1, with an additional term measuring the distance between the trajectories of virtual particles and N_m filtered trajectories.

$$j_4(z_b) \;=\; j_1(z_b) \;+\; \frac{\alpha_t}{2} \sum_{j=1}^{N_m} \int_0^T \left| X_j(t) - X_j^m(t) \right|^2 \, dt \qquad (19)$$

As described in Section 7.2, we have $N_m = 200$. For the weight parameters, we choose $\alpha_t = 2 \times 10^{-5}$ and $\alpha_p = 10^{-3}$. Figure 10 (a) shows a substantial improvement in the quality of topography identification. Unlike the case with unfiltered trajectories, the value of the diagnostic function j_{tot} regularly decreases all along the minimization process. Finally, it is divided by 37 with respect to its initial value.
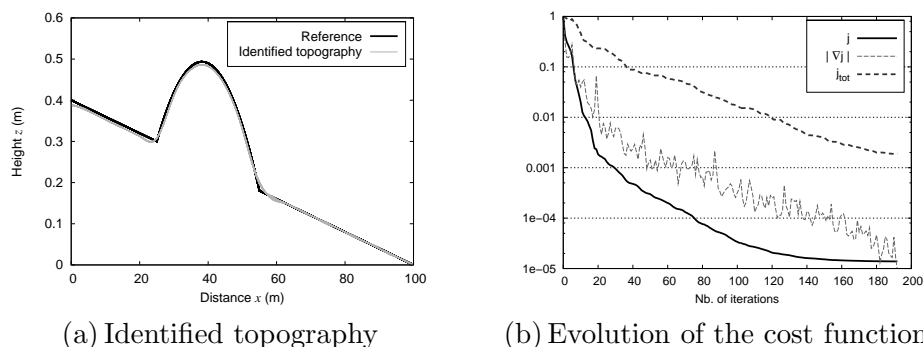

(a) Identified topography　　　　(b) Evolution of the cost function

Figure 8: Identification of the topography using water depth measurements and reference trajectories. $\alpha_t = 10^{-5}$, $\alpha_p = 10^{-4}$.
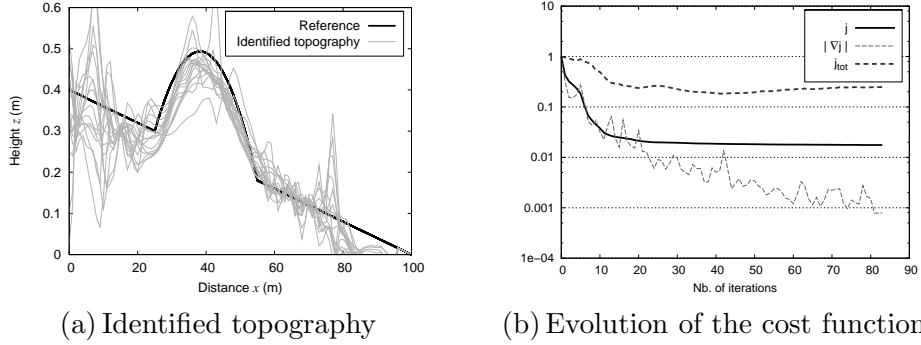
(a) Identified topography

(b) Evolution of the cost function

Figure 9: Identification of the topography using water depth measurements and perturbed trajectories. $\alpha_t = 10^{-5}$, $\alpha_p = 10^{-4}$.

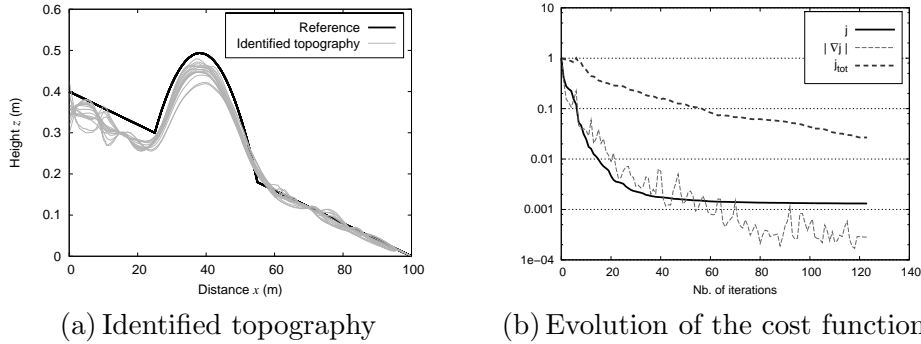(a) Identified topography

(b) Evolution of the cost function

Figure 10: Identification of the topography using water depth measurements and filtered trajectories. $\alpha_t = 2 \times 10^{-5}$, $\alpha_p = 10^{-3}$.

7.5 Joint identification of topography and initial conditions

We now seek to identify jointly the topography z_b and the initial conditions (water depth h_0 and velocity $\mathbf{u}_0$) using the available observations from the initial assumption on both parameters. Like in Section 7.4, we make the *a priori* hypothesis that the bed is made of a longitudinal slope of 0.4% without bump. However, regarding the initial condition, we use the steady state obtained with the modified topography instead of the reference one.

7.5.1 Water depth measurements

We first try to identify the topography using only water depth measurements h_i^{obs} at the abscissae $x_1 = 15\,m$ and $x_2 = 70\,m$. The corresponding cost function is the following

When using only water depth measurements as observations for the identification of topography and initial conditions, the cost function is similar to j_1 in section 7.4.1. The only difference is that the initial condition h_0 and $\mathbf{u}_0$ are now control variables. The new

16

cost function can then be written as

$$j_5(z_b, h_0, \mathbf{u}_0) \ = \ \frac{1}{2} \sum_{i=1}^{2} \int_0^T \int_0^{y_{max}} \left\| h(x_i, y; t) - h_i^{obs}(y; t) \right\|^2 dy \, dt \ + \ \frac{\alpha_p}{2} \left\| \nabla z_b \right\|^2 \tag{20}$$

The weight for the regularization term is set to $\alpha_p = 10^{-4}$. One can see in Figure 11 (a)

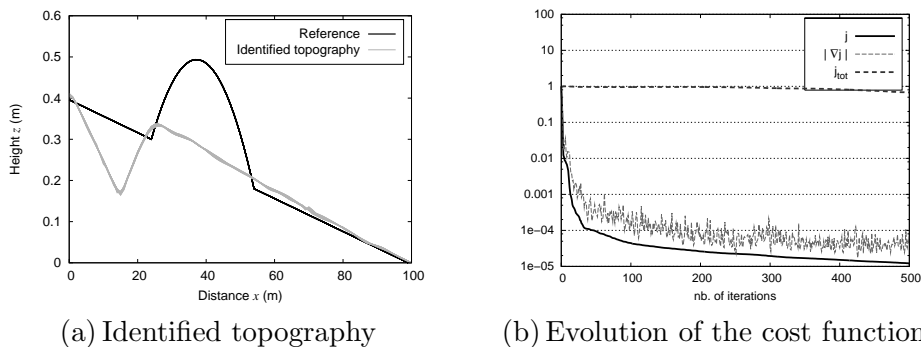(a) Identified topography (b) Evolution of the cost function

Figure 11: Joint identification of the topography and the initial conditions using water depth measurements. $\alpha_p = 10^{-4}$.

that the use of water depth measurements only is far from being sufficient for the identification of the topography together with the initial conditions. The identified topography is very different from the reference, just as the initial conditions not represented here. The diagnostic function j_{tot} is barely divided by 2.

7.5.2 Observation of filtered trajectories

Finally, we use the filtered trajectories X_j^m as observations in addition to the water depth measurements for the joint identification of topography and initial conditions. The cost function is built from j_5, with an additional term measuring the distance between the trajectories of virtual particles and N_m filtered trajectories.

$$j_6(z_b, h_0, \mathbf{u}_0) \ = \ j_5(z_b, h_0, \mathbf{u}_0) \ + \ \frac{\alpha_t}{2} \sum_{j=1}^{N_m} \int_0^T \left| X_j(t) - X_j^m(t) \right|^2 dt \tag{21}$$

The weight given to the observations of trajectories is set to $\alpha_t = 10^{-4}$ while the one for the regularization term is set to $\alpha_p = 8 \times 10^{-3}$. As shown in Figure 12 (a), the identified topography is close to the reference, with a good recovery of the bump. It is similar to the result in section 7.4.4. As for the initial conditions, we can see in Figure 12 (c) and (d) that it reproduce the same main features as the reference. However, we can notice irregular variations in the identified variables in the upper part of the flow, as well as a

(a) Identified topography

(b) Evolution of the cost function
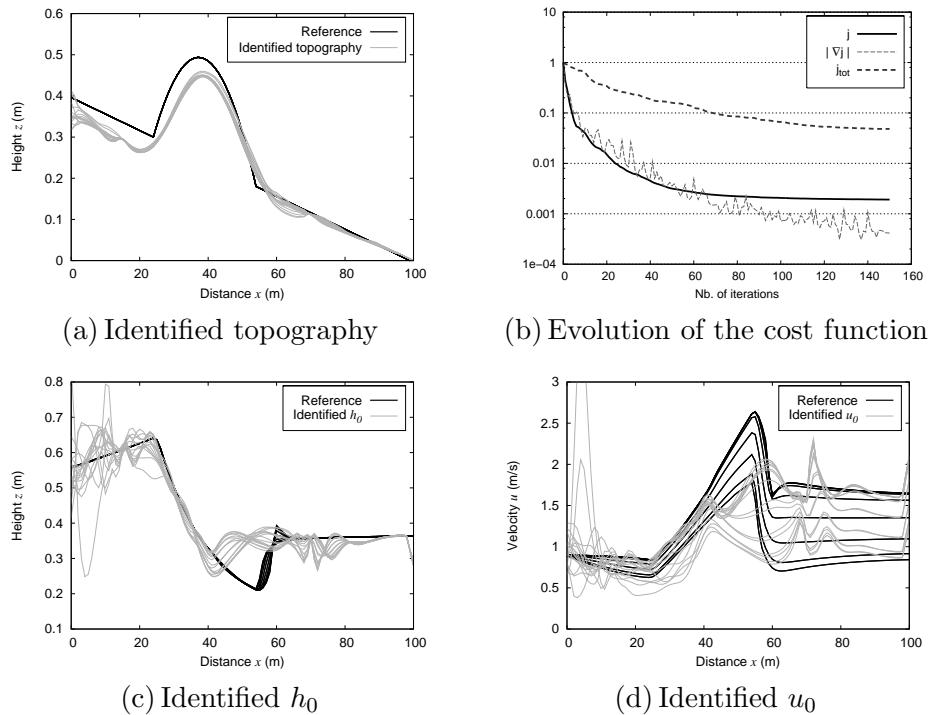
(c) Identified h_0

(d) Identified u_0

Figure 12: Joint identification of the topography and the initial conditions using water depth measurements and filtered trajectories. $\alpha_t = 1 \times 10^{-4}$, $\alpha_p = 8 \times 10^{-3}$.

slight over-estimation of the water depth combined with a slight underestimation of the longitudinal velocity in the area just downstream from the bump.

The value of the diagnostic function j_{tot} is divided by about 20 at the end of the optimization process with respect to its initial value.

8 CONCLUSION

We have presented a method to include lagrangian observations into a data assimilation framework in order to improve the identification of control variables for a river hydraulics model based on the shallow water equations. The link between the eulerian state variables from the shallow water model and the lagrangian observations of particle trajectories is made thanks to a transport model. Numerical twin data assimilation experiments demonstrate that this method makes it possible to significantly improve the identification of bed elevation and initial conditions in an academic configuration.

A simple spatio-temporal filter has been successfully used to improve the quality of the identification with trajectories observations transported by a velocity field with small-scale perturbations. In reality, however, physical phenomena that affect the free surface are more complex and a better surface velocity model should be very beneficial to an application of this method to real river flows.

REFERENCES

[1] F.-X. Le Dimet and O. Talagrand. Variational algorithms for analysis and assimilation of meteorological observations: theoretical aspects, *Tellus, 38A,* 97–110, (1986).

[2] J.-C. Gilbert and C. Lemaréchal. Some numerical experiments with variable storage quasi-Newton algorithms, *Mathematical programming, 45,* 407–435, (1989).

[3] E.F. Toro. *Shock-capturing methods for free-surface shallow flows,* J. Wiley and Sons, (2001).

[4] L. Hascoët and V. Pascual. TAPENADE 2.1 user's guide, Technical Report RT–300, INRIA, (2004).

[5] J.-L. Lions. *Optimal control of systems governed by partial differential equations,* Springer-Verlag, (1971).

[6] A. Griewank. *Evaluating Derivatives: Principles and Techniques of Algorithmic Differentiation, Frontiers in Appl. Math., SIAM,* vol. 19, Philadelphia, PA, (2000).

[7] M. Honnorat, F.-X. Le Dimet, Y. Loukili and J. Monnier. DASSFLOW : a direct and adjoint model for 2D Shallow Water flows, Research report RR–5756, INRIA, (2005).